Convex relaxation approaches for high dimensional optimal transport

Yuehaw Khoo ^{*}, Tianyun Tang [†] November 19, 2025

Abstract

Optimal transport (OT) is a powerful tool in mathematics and data science but faces severe computational and statistical challenges in high dimensions. We propose convex relaxation approaches based on marginal and cluster moment relaxations that exploit locality and correlative sparsity in the distributions. These methods approximate high-dimensional couplings using low-order marginals and sparse moment statistics, yielding semidefinite programs that provide lower bounds on the OT cost with greatly reduced complexity. For Gaussian distributions with sparse correlations, we prove reductions in both computational and sample complexity, and experiments show the approach also works well for non-Gaussian cases. In addition, we demonstrate how to extract transport maps from our relaxations, offering a simpler and interpretable alternative to neural networks in generative modeling. Our results suggest that convex relaxations can provide a promising path for dimension reduction in high-dimensional OT.

1 Introduction

1.1 Optimal transport

In this paper, we consider the following optimal transport (OT) problem:

$$\inf_{\pi} \left\{ \int_{\mathcal{X} \times \mathcal{Y}} c(x, y) d\pi(x, y) : \ \pi \in \Pi(\mu, \nu) \right\}, \tag{OT}$$

where $d \in \mathbb{N}^+$, μ and ν are probability measures on Borel sets $\mathcal{X}, \mathcal{Y} \subset \mathbb{R}^d$, $c : \mathcal{X} \times \mathcal{Y} \to \mathbb{R}^+$ is a lower semi-continuous cost function, and $\Pi(\mu, \nu)$ denotes the set of joint probability measures on $\mathcal{X} \times \mathcal{Y}$ with marginals μ and ν (the so-called transport plans).

Originating in the works of Monge and Kantorovich [23, 35], this problem has grown into a powerful mathematical framework with deep ties to analysis, geometry, partial differential equations, and optimization [8, 12, 17, 44, 50, 51]. Beyond pure mathematics, OT has become a central tool in applications across the sciences. In machine learning and data

^{*}Department of Statistics, University of Chicago, (ykhoo@uchicago.edu). The research of this author is partially funded by NSF DMS-2339439, DOE DE-SC0022232, DARPA The Right Space HR0011-25-9-0031, and a Sloan research fellowship.

[†]Department of Statistics, University of Chicago, (ttang@u.nus.edu).

science, it plays a key role through the Wasserstein distance, which measures similarity between probability distributions while respecting their underlying geometry. This geometric viewpoint has enabled advances in generative modeling [4, 5, 11, 18, 47]. Compared to divergences such as the Kullback–Leibler divergence [28], OT-based methods often lead to more stable training and are better at handling distributions with disjoint supports [42].

1.2 Curse of dimensionality

Despite its promise, applying OT in high dimensions remains difficult. The computational cost grows quickly with dimension, and the number of samples needed to estimate OT scales exponentially [15,16,53]. This creates a major obstacle for large-scale machine learning and data science, where data often lie in very high-dimensional spaces. To mitigate this, several dimension-reduction strategies have been proposed.

One popular approach is to use neural network parameterizations of transport maps or of the Kantorovich potentials (the dual variables in OT) [27, 33, 34]. These methods are widely applied in generative modeling, but their training involves non-convex optimization and thus lacks strong theoretical guarantees.

Another strategy is the *sliced Wasserstein* distance, which computes one-dimensional OT along random (or learned) projections and then averages the results [6,32,38,43]. This substantially reduces computational cost, though the resulting distance is generally different from the true Wasserstein distance.

A further line of work [22, 49, 54] leverages the smoothness of the distributions to obtain statistical rates for Wasserstein distance and transport map estimation that avoid exponential dependence on dimension. However, these improvements require strong regularity assumptions and often involve high computational complexity, limiting their use in large-scale applications.

1.3 Our contributions

In this paper, to address the high dimensionality of (OT), we make the following contributions:

- We introduce convex relaxations of (OT) that approximate high-dimensional distributions using only sparse collections of low-order marginals or cluster moments. The resulting semidefinite programs provide computable lower bounds on the OT cost.
- For Gaussian models with sparse correlations, we prove that our method reduces both computational and sample complexity.
- Beyond the Gaussian setting, numerical experiments show that our approach remains
 effective for non-Gaussian distributions and can be used to extract transport maps
 for generative modeling.

Marginal relaxation has a long history in areas such as graphical models, density functional theory, and statistical physics [2, 39, 52], where it is commonly applied to complex many-body systems. In this work, we adapt the idea to optimal transport by applying it to the joint distribution $\pi(x, y)$, with both marginals μ and ν prescribed. Related work by

Khoo et al. [24,25] introduced marginal relaxation techniques for *multi-marginal* OT, where the difficulty comes from coupling N low-dimensional variables. In contrast, our setting involves only two variables, but each lies in a very high-dimensional space. While the sliced Wasserstein distance also relies on low-order marginals to define a tractable distance, our approach is designed to closely approximate the original Wasserstein distance.

In [36], Mula and Nouy proposed sum-of-squares (SOS) moment relaxations [29, 30] of (OT), which approximate high-dimensional distributions through low-order statistics. Their method avoids spatial discretization, making it particularly suitable for (OT) between continuous distributions. Our cluster moment relaxation is inspired their approach. However, we realize that their method do not scale well in high-dimensional setting, because one has to solve a semidefinite program (SDP) of size $\binom{2d+n}{n}$, where n is the relaxation degree—a combinatorial growth that quickly becomes memory-prohibitive for large d and n. In contrast, our cluster moment relaxation leverages the local structure of (OT) and requires only a sparse collection of moments, resulting in much smaller SDP blocks and computations that remain tractable even in high dimensions.

Another related work is by Vacher and Bach [49], who use sum-of-squares representations of kernel functions in the dual (Kantorovich) formulation of (OT) to model smooth nonnegative functions. Their method, however, requires the underlying distributions to be smooth. By contrast, our cluster moment relaxation also applies to non-smooth settings, including singular cases such as Dirac measures.

1.4 Organization

The rest of the paper is organized as follows. Section 2 introduces our convex relaxation approaches for (OT). Section 3 provides a theoretical analysis of the cluster moment relaxation in the Gaussian setting. In Section 4, we describe how to extract transport maps from the relaxation. Section 5 presents numerical experiments that illustrate the effectiveness of our methods. Section 6 concludes with a brief summary and discussion. Detailed proofs of the theoretical results are given in Appendix A.

2 Convex relaxations

In this section, we propose a convex relaxation framework for (OT). To formally introduce the relaxation approaches, we first present the relevant notations, definitions, and assumptions in the following subsection. For intuition, readers may also refer to Figures 1–2.

2.1 Preliminaries

In what follows, we introduce the basic notation and structures that support our convex relaxation framework. Definition D1 sets up index partitions and the associated product spaces. Definition D2 introduces moments of probability measures. Definition D3 uses graphs to encode sparsity patterns and correlation structure. Finally, Definition D4 defines projection operators for extracting marginals and moments.

D1 (indices, partitions, marginals) For any integer $n \in \mathbb{N}^+$, define sets $[n] := \{1, 2, \dots, n\}$ and

$$[n]_2 := \{ ij : i, j \in \mathbb{N}^+, \ 1 \le i < j \le n \}.$$
 (1)

Fix $K \in \mathbb{N}^+$. Partition x and y into K clusters $(x_1; x_2; \ldots; x_K)$ and $(y_1; y_2; \ldots; y_K)$, where each cluster may contain multiple variables. We do not require x_k and y_k to share the same coordinates in x and y. For each $k \in [K]$, let \mathcal{X}_k and \mathcal{Y}_k denote the Borel subsets of \mathcal{X} and \mathcal{Y} corresponding to clusters x_k and y_k , respectively. Then

$$\mathcal{X} = \mathcal{X}_1 \times \mathcal{X}_2 \times \cdots \times \mathcal{X}_K, \qquad \mathcal{Y} = \mathcal{Y}_1 \times \mathcal{Y}_2 \times \cdots \times \mathcal{Y}_K.$$
 (2)

For simplicity, we write

$$z = (x, y), \quad \mathcal{Z} = \mathcal{X} \times \mathcal{Y}, \quad z_k = (x_k, y_k), \quad \mathcal{Z}_k = \mathcal{X}_k \times \mathcal{Y}_k$$
 (3)

The marginals of μ and ν on \mathcal{X}_k and \mathcal{Y}_k are denoted by μ_k and ν_k . The marginals of μ and ν on $\mathcal{X}_i \times \mathcal{X}_j$ and $\mathcal{Y}_i \times \mathcal{Y}_j$ are denoted by μ_{ij} and ν_{ij} .

D2 (measures, moments)

Let \mathcal{Z} be a Borel set in a Euclidean space. Denote by $\mathcal{M}(\mathcal{Z})$ the space of signed Borel measures on \mathcal{Z} satisfying $\eta(\mathcal{Z}) = 1$ for any $\eta \in \mathcal{M}(\mathcal{Z})$, and by $\mathcal{P}(\mathcal{Z})$ the subset of probability measures on \mathcal{Z} , i.e.,

$$\mathcal{P}(\mathcal{Z}) := \{ \eta \in \mathcal{M}(\mathcal{Z}) : \eta \ge 0 \}. \tag{4}$$

For $\eta \in \mathcal{P}(\mathcal{Z})$ and a measurable function $\Xi : \mathcal{Z} \to \mathbb{R}^{m \times n}$, we define the corresponding moment as

$$\eta(\Xi) := \int_{\Xi} \Xi(z) \, \mathrm{d}\eta(z). \tag{5}$$

When Ξ is vector- or matrix-valued, the integral in (5) is understood to be taken elementwise.

D3 (graphs)

For a graph G, let V(G) and E(G) denote its vertex and edge sets, respectively. Throughout this paper, all graphs are assumed to be undirected and loop-free. Whenever we write $ij \in E(G)$, we implicitly assume that i < j.

We introduce a reference graph \mathcal{G} with vertex set $V(\mathcal{G}) = [K]$, which serves as the underlying structure for the convex relaxation methods developed in this work. Without loss of generality, we further assume that \mathcal{G} is connected, since otherwise our models can be decomposed into independent subproblems, each associated with a connected underlying structure.

Define \mathbb{S}^d to be the set of d by d symmetric real matrices. For any graph $G=([d],\mathcal{E})$ Define the sets

$$\mathbb{S}(G,0) := \{ X \in \mathbb{S}^d : X_{ij} = 0 \text{ for all } i \neq j \text{ with } ij \notin \mathcal{E} \},$$
 (6)

$$\mathbb{S}(G,c) := \{ X \in \mathbb{S}^d : X_{ij} = 0 \text{ whenever } i = j \text{ or } ij \in \mathcal{E} \}.$$
 (7)

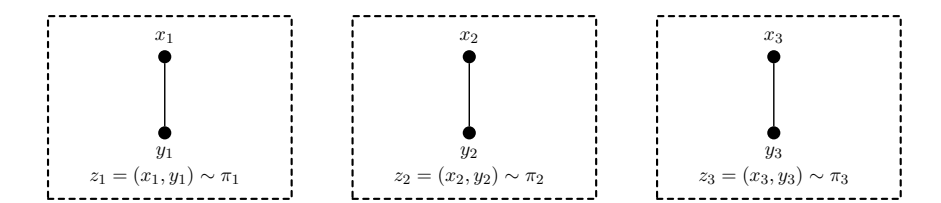


Figure 1: Step 1. Partition x and y into K clusters $(x_1; x_2; \dots; x_K)$ and $(y_1; y_2; \dots; y_K)$. Construct a local coupling within each cluster: $z_k = (x_k, y_k) \sim \pi_k$. The mean-field approximation $\bigotimes_{k=1}^K \pi_k$ of π is exact if the z_k 's are independent.

See the following example:

$$G: \bullet - \bullet - \bullet \qquad \mathbb{S}(G,0) := \left\{ \begin{bmatrix} a & b & 0 \\ b & c & d \\ 0 & d & e \end{bmatrix} \right\}, \quad \mathbb{S}(G,c) := \left\{ \begin{bmatrix} 0 & 0 & f \\ 0 & 0 & 0 \\ f & 0 & 0 \end{bmatrix} \right\}$$
(8)

We say that G is a sparsity pattern of A if $A \in \mathbb{S}(G,0)$. For any $A \in \mathbb{S}^d$, we write $[A]_{G,0} := \operatorname{Proj}_{\mathbb{S}(G,0)}(A)$ and $[A]_{G,c} := \operatorname{Proj}_{\mathbb{S}(G,c)}(A)$.

For any $h \in \mathbb{N}$, we define graph G^h connecting nodes within graph distance h in G, that is

$$\forall ij \in [d]_2, \ ij \in E(G^h), \ \text{if and only if } \operatorname{dist}_G(i,j) \le h.$$
 (9)

We will use it to encode correlation radius. See the following example:

$$G: \bullet - \bullet - \bullet - \bullet - G^2: \bullet - \bullet - \bullet - (10)$$

D4 (projection operators)

Through this this paper, we use two projection operators $P(\cdot)$ and $R(\cdot)$ defined as

(i) P_u (probability measure)=marginal measure on u. For example, let $(u_2, u_3) \sim \eta$

$$P_{(u_1,u_2)}(\eta)$$
 is the marginal of η on u_2 . (11)

(ii) R_u (collection of functions)=functions of u. For example,

$$R_x \begin{pmatrix} \begin{bmatrix} xy & 1 \\ x^2 & y \end{bmatrix} \end{pmatrix} = \begin{bmatrix} 1 \\ x^2 \end{bmatrix}, \qquad R_y \begin{pmatrix} \begin{bmatrix} xy & 1 \\ x^2 & y \end{bmatrix} \end{pmatrix} = \begin{bmatrix} 1 \\ y \end{bmatrix}, \tag{12}$$

2.2 Marginal relaxation

In this subsection, we present the marginal relaxation of (OT), which approximates the high-dimensional transport plan in two steps, illustrated in Figures 1–2. Step 1 groups strongly correlated variables and constructs local couplings within each group. Step 2 introduces pairwise couplings across groups.

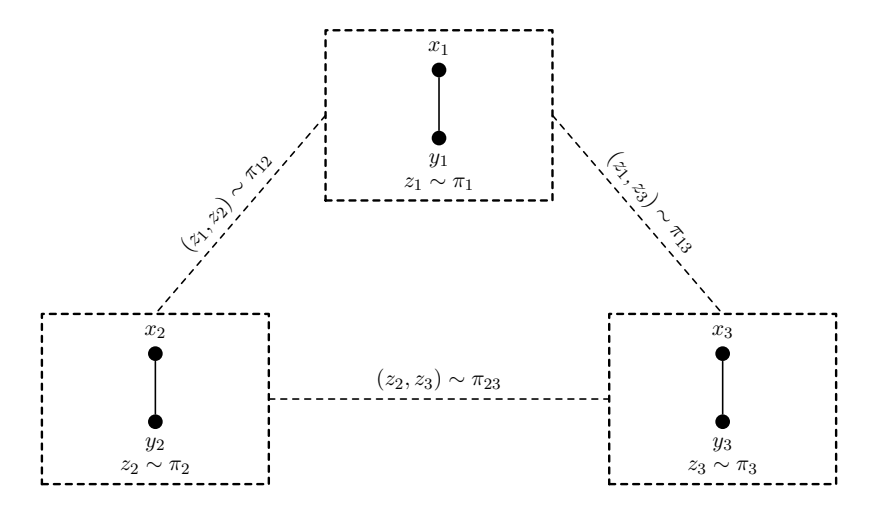


Figure 2: Step 2. Add pairwise couplings between correlated clusters: $(z_i, z_j) \sim \pi_{ij}$, consistent with marginals $P_{z_i}(\pi_{ij}) = \pi_i$, $P_{z_j}(\pi_{ij}) = \pi_j$ and satisfying the PSD constraint (15). In this example, the reference graph \mathcal{G} (Definition D3) is a triangle.

The problem (OT) can be equivalently written as follows

$$\inf_{\pi} \pi(c) \tag{OT}$$

s.t.
$$P_x(\pi) = \mu$$
, $P_y(\pi) = \nu$ (1a)

$$\pi \in \mathcal{P}(\mathcal{Z}).$$
 (1b)

We will relax the above conditions (1a) and (1b) as some conditions on the marginals of π .

• OT marginal constraints: We relax the marginal constraint (1a) as the following conditions on π_{ij}

$$P_x(\pi_{ij}) = \mu_{ij}, \qquad P_y(\pi_{ij}) = \nu_{ij}. \tag{13}$$

We will later restrict the marginal constraints in a reference graph \mathcal{G} defined in Definition D3.

• Local positivity: We relax the positivity of π as the positivity of its marginals:

$$\pi_{ij} \in \mathcal{P}(\mathcal{Z}_i \times \mathcal{Z}_j).$$
 (14)

Note that the positivity of π_i and π_j will be implicit implied by (14) and the consistency condition discussed later.

• Global positivity: We relax the nonnegativity constraint (1b) as the positive semidefiniteness (PSD) condition on the marginals $(\pi_k, \pi_{ij})_{[K], [K]_2}$. This means that for any family of square-integrable functions $(f_k)_{[K]} \in (L^2(\pi_k))_{[K]}$ the following inequality holds

$$\sum_{k \in [K]} \pi_k \left(f_k^2 \right) + \sum_{ij \in [K]_2} 2\pi_{ij} (f_i f_j) = \pi \left(\left(\sum_{k \in [K]} f_k(z_k) \right)^2 \right) \ge 0, \tag{15}$$

which comes from the linearity of integration as well as the fact that $(\pi_k, \pi_{ij})_{[K],[K]_2}$ are 1 and 2 marginals of the probability measure π . We use " $(\pi_k, \pi_{ij})_{[K],[K]_2} \succeq 0$ " to denote the condition (15). When the sets \mathcal{Z}_k are finite, condition (15) is equivalent to requiring the block matrix

$$\begin{bmatrix} \operatorname{Diag}(\pi_{1}) & \pi_{12} & \cdots & \pi_{1K} \\ \pi_{12}^{\top} & \operatorname{Diag}(\pi_{2}) & \ddots & \pi_{2K} \\ \vdots & \ddots & \ddots & \vdots \\ \pi_{1K}^{\top} & \pi_{2K}^{\top} & \cdots & \operatorname{Diag}(\pi_{K}) \end{bmatrix} \succeq 0, \tag{16}$$

where $\text{Diag}(\pi_k)$ denotes a diagonal matrix with diagonal entries being π_k . The PSD condition is often used to strengthen marginal relaxations, with applications in density functional theory [9, 10, 25, 40].

• Consistency: We relax the condition that π_k, π_{ij} are one- and two-marginals of π into some local consistency conditions. For every $ij \in [K]_2$, the marginals of π_{ij} agree with those of π_i and π_j . The conditions are summarized as follows:

$$P_{z_i}(\pi_{ij}) = \pi_i, \qquad P_{z_j}(\pi_{ij}) = \pi_j, \tag{17}$$

where P_{z_i} , P_{z_j} are defined in Definition D4.

With the above conditions on the one- and two-marginals π_k, π_{ij} of π in (OT), we are now able to present the marginal relaxation of (OT). Suppose c(z) has the following decomposition

$$c(z) = \sum_{k \in [K]} c_k(z_k). \tag{18}$$

The marginal relaxation of (OT) is as follows:

$$\inf_{(\pi_k, \pi_{ij})_{[K], [K]_2}} \sum_{k \in [K]} \pi_k(c_k) \tag{OT_{mar}}$$

s.t.
$$P_x(\pi_{ij}) = \mu_{ij}$$
, $P_y(\pi_{ij}) = \nu_{ij}$, $\forall ij \in E(\mathcal{G})$ (2a)

$$P_{z_i}(\pi_{ij}) = \pi_i, \quad P_{z_j}(\pi_{ij}) = \pi_j, \quad \forall ij \in [K]_2$$
 (2.1b)

$$\pi_{ij} \in \mathcal{P}(\mathcal{Z}_i \times \mathcal{Z}_j), \quad \forall ij \in [K]_2$$
 (2.2b)

$$(\pi_k, \pi_{ij})_{[K], [K]_2} \succeq 0,$$
 (2.3b)

where the constraint (2a) is a relaxation of (1a) and (2.1b)–(2.3b) are relaxations of (1b). Note that the condition $\pi_k \in \mathcal{P}(\mathcal{Z}_k)$ is implied by (2.1b) so we omit it to avoid redundancy. The reference graph \mathcal{G} , first mentioned in Definition D3 (it is a triangle in Figure 2), controls which pairwise marginals are retained. Although the complete graph $(E(\mathcal{G}) = [K]_2)$ gives the tightest relaxation, sparser graphs can reduce computational complexity for solving the SDP problem, which will be elaborated later.

Compared to (OT), whose decision variable is a full d-dimensional measure, this formulation works only with low-dimensional marginals, drastically reducing complexity. For

example, when K = d and $\mathcal{X}_k = \mathcal{Y}_k = [r]$, (OT) involves r^{2d} variables, while (OT_{mar}) involves only $r^4d(d-1)/2 + r^2d$.

From (2.2b) and (2.3b), the matrix variable in (16) (in the finite setting) is both PSD and nonnegative. In this case, the problem (OT_{mar}) is a doubly-nonnegative (DNN) programming problem. Although it is computational tractable with several solvers [20,21,45] available, high dimensional DNN problems are still challenging due to its large number of variables and constraints. To reduce the dimensionality of (OT_{mar}), we further relax its constraints in the following two ways:

The first way is to drop the PSD condition (2.3b) of (OT_{mar}) , obtaining the following problem:

$$\inf_{(\pi_k, \pi_{ij})_{[K], E(\mathcal{G})}} \sum_{k \in [K]} \pi_k(c_k) \tag{OT}_{\text{mar}}^1)$$

s.t.
$$P_x(\pi_{ij}) = \mu_{ij}$$
, $P_y(\pi_{ij}) = \nu_{ij}$, $\forall ij \in E(\mathcal{G})$ (3a)

$$P_{z_i}(\pi_{ij}) = \pi_i, \quad P_{z_i}(\pi_{ij}) = \pi_j, \quad \forall ij \in E(\mathcal{G})$$
 (3.1b)

$$\pi_{ij} \in \mathcal{P}(\mathcal{Z}_i \times \mathcal{Z}_j), \quad \forall ij \in E(\mathcal{G}).$$
 (3.2b)

In (OT_{mar}^1) , we only include π_{ij} on the edge set of $E(\mathcal{G})$. This is because for any $ij \in [K]_2 \setminus E(\mathcal{G})$, we may define π_{ij} to be the product measure $\pi_i \otimes \pi_j$ and it is easy to check that $(\pi_k, \pi_{ij})_{[K], [K]_2}$ satisfy all the constraints in (OT_{mar}) except the PSD constraint (2.3b). Therefore, by dropping the PSD, we also dropped a large number of unrelated decision variables if \mathcal{G} is sparse. In addition, the problem (OT_{mar}^1) is a linear programming (LP) problem, which is much easier than SDP.

The second way is to remove the nonnegativity constraint (2.2b) from (OT_{mar}) , obtaining the following problem:

$$\inf_{(\pi_k, \pi_{ij})_{[K], [K]_2}} \sum_{k \in [K]} \pi_k(c_k) \tag{OT}_{\text{mar}}^2)$$

s.t.
$$P_x(\pi_{ij}) = \mu_{ij}$$
, $P_y(\pi_{ij}) = \nu_{ij}$, $\forall ij \in E(\mathcal{G})$ (4a)

$$P_{z_i}(\pi_{ij}) = \pi_i, \quad P_{z_j}(\pi_{ij}) = \pi_j, \quad \forall ij \in [K]_2$$
 (4.1b)

$$\pi_{ij} \in \mathcal{M}(\mathcal{Z}_i \times \mathcal{Z}_j), \quad \forall ij \in [K]_2$$
 (4.2b)

$$(\pi_k, \pi_{ij})_{[K], [K]_2} \succeq 0.$$
 (4.3b)

Remark 2.1. The problem (OT_{mar}^2) is an SDP without nonnegativity constraints. Its dimension can be further reduced via the *chordal conversion* method in [46]. For example, consider the setting K = d and $\mathcal{X}_k = \mathcal{Y}_k = [r]$. Then $\pi_k \in \mathbb{R}^{r^2}$ and $\pi_{ij} \in \mathbb{R}^{r^2 \times r^2}$. The constraint (4.1b) becomes

$$\pi_{ij} \mathbf{1}_{r^2} = \pi_i, \qquad \pi_{ij}^{\top} \mathbf{1}_{r^2} = \pi_j.$$
 (19)

These conditions can be compactly written as

$$X(I_d \otimes \mathbf{1}_{r^2} - J_d \otimes \mathbf{1}_{r^2}) = 0, \tag{20}$$

where X is the matrix in (16), I_d is the identity matrix, and J_d is the cyclic shift matrix with $J_{2,1} = J_{3,2} = \cdots = J_{d,d-1} = J_{1,d} = 1$ and all other entries zero. Since $X \succeq 0$, (20) is equivalent to

$$\langle X, HH^{\top} \rangle = 0,$$
 (21)

with $H = (I_d \otimes \mathbf{1}_{r^2} - J_d \otimes \mathbf{1}_{r^2})$. Thus, (20) reduces to a single affine constraint on X. Noting that $\operatorname{rank}(HH^{\top}) = \operatorname{rank}(H) = d - 1$, this constraint involves a low-rank coefficient matrix.

The remaining linear constraints in (OT_{mar}^2) and the linear objective involve only the diagonal blocks $Diag(\pi_k)$ or the off-diagonal blocks $\pi_{ij}, \pi_{ij}^{\mathsf{T}}$ for $ij \in E(\mathcal{G})$. This yields a sparse plus low-rank structure [46, Definition 1.1], which enables significant dimensionality reduction. For instance, if \mathcal{G} is a tree, [46, Theorem 1.4] shows that (OT_{mar}^2) decomposes into a multi-block SDP with block size at most $r^2 + 2d$, far smaller than the ambient dimension dr^2 . For general \mathcal{G} , the block size is related to the tree-width of \mathcal{G} . Please see [46, Section 2] for more details about tree-width.

While the marginal relaxation already reduces dimensionality significantly, it still works directly with measures, which becomes costly in continuous domains. To address this, we next introduce the cluster moment relaxation, which works with moments instead of full measures.

2.3 Cluster moment relaxation

In this subsection, we introduce the cluster moment relaxation, which applies moment relaxation to the marginal relaxations (OT_{mar}^1) , (OT_{mar}^1) and (OT_{mar}^2) of (OT). Following the methodology of [9], we begin by defining the cluster basis.

Fix a relaxation degree $n \in \mathbb{N}^+$, specifying the maximum polynomial degree retained. Let $\{\phi_j : \mathbb{R} \to \mathbb{R}\}_{j=0}^n$ be basis functions with $\phi_0 \equiv 1$ (e.g., $\phi_j(s) = s^j$). For any multi-index $\alpha = (\alpha_1, \ldots, \alpha_{2K}) \in \mathbb{N}^{2d}$, define

$$\phi_{\alpha} := \prod_{k \in [K]} \phi_{\alpha_k}(x_k) \,\phi_{\alpha_{k+K}}(y_k). \tag{22}$$

If x_k (or y_k) contains multiple coordinates, then α_k is itself a multi-index, and $\phi_{\alpha_k}(x_k)$ denotes the product $\prod_i \phi_{\alpha_k[i]}(x_k[i])$, where $\alpha_k[i]$ and $x_k[i]$ are the respective coordinates. We define the *cluster basis* for z_k , as:

$$\Phi_k := \{ \phi_\alpha : \phi_\alpha \text{ only has variables in } z_k, \ |\alpha| \le n \},$$
 (23)

which can be viewed as vectors of basis functions supported on the variables z_k , up to degree n. If c_k lies in the span of $\Phi_k \Phi_k^{\top}$, it can be written as

$$c_k(z_k) = \langle C_k, \Phi_k \Phi_k^{\top} \rangle \tag{24}$$

for some symmetric matrix C_k . The objective of the relaxation then becomes

$$\sum_{k \in [K]} \langle C_k, M_k \rangle, \quad \text{where} \quad M_k := \pi_k(\Phi_k \Phi_k^\top), \quad M_{ij} := \pi_{ij}(\Phi_i \Phi_j^\top). \tag{25}$$

Here M_k is a Gram-type moment matrix and therefore always symmetric positive semidefinite, while M_{ij} collects cross-moments between cluster basis and need not be symmetric or positive semidefinite.

We next describe the constraints that these moment matrices must satisfy. They mirror the marginal/local and global positivity/consistency constraints from (OT_{mar})

• **OT marginal constraints:** We relax the marginal constraints in (13) using moments of the x and y marginal. In detail, let

$$M_k^x := \pi_k \left(\mathbf{R}_x \left(\Phi_k \Phi_k^{\top} \right) \right), \qquad M_k^y := \pi_k \left(\mathbf{R}_y \left(\Phi_k \Phi_k^{\top} \right) \right).$$
 (26)

$$M_{ij}^{x} := \pi_{ij} \left(\mathbf{R}_{x} \left(\Phi_{i} \Phi_{j}^{\top} \right) \right), \qquad M_{ij}^{y} := \pi_{ij} \left(\mathbf{R}_{y} \left(\Phi_{i} \Phi_{j}^{\top} \right) \right).$$
 (27)

We have that

$$M_k^x = \mu \left(\mathbf{R}_x \left(\Phi_k \Phi_k^{\top} \right) \right), \qquad M_k^y = \nu \left(\mathbf{R}_y \left(\Phi_k \Phi_k^{\top} \right) \right),$$
 (28)

$$M_{ij}^{x} = \mu \left(\mathbf{R}_{x} \left(\Phi_{i} \Phi_{j}^{\top} \right) \right), \qquad M_{ij}^{y} = \nu \left(\mathbf{R}_{y} \left(\Phi_{i} \Phi_{j}^{\top} \right) \right),$$
 (29)

which means that some entries of the moment matrices M_k , M_{ij} are prescribed as the moments of μ and ν .

• Local positivity: The local positivity condition (14) in marginal relaxation is relaxed as the following condition on the moment matrices

$$(M_i, M_j, M_{ij}) \in \mathcal{C}_{ij}, \tag{30}$$

where C_{ij} is a convex set encoding necessary conditions for (M_i, M_j, M_{ij}) to represent the moments of some probability measure π_{ij} . The conditions can be summarized as that: (M_i, M_j, M_{ij}) is embedded in a PSD matrix defined by sum-of-squares (SOS) hierarchy $\pi_{ij}(SOS \text{ for } (z_i, z_j)) \geq 0$. In the marginal, this is enforced by point-wise nonnegativity.

• Global positivity: We relax the global positivity condition (15) in (OT_{mar}) by restricting the test functions f_k to the form $f_k = v_k^{\mathsf{T}} \Phi_k$ for some vector v_k . Substituting into (15) gives

$$0 \leq \sum_{k \in [K]} \pi_k \Big((v_k^{\top} \Phi_k)^2 \Big) + \sum_{ij \in [K]_2} 2\pi_{ij} \Big((v_i^{\top} \Phi_i) (v_j^{\top} \Phi_j) \Big)$$

$$= \sum_{k \in [K]} v_k^{\top} M_k v_k + \sum_{ij \in [K]_2} 2v_i^{\top} M_{ij} v_j.$$
(31)

Since this inequality must hold for all choices of $(v_k)_{k\in[K]}$, it is equivalent to requiring the block moment matrix

$$M := \begin{bmatrix} M_1 & M_{12} & \cdots & M_{1K} \\ M_{12}^{\top} & M_2 & \ddots & M_{2K} \\ \vdots & \ddots & \ddots & \vdots \\ M_{1K}^{\top} & M_{2K}^{\top} & \cdots & M_K \end{bmatrix} \succeq 0.$$
 (32)

• Consistency: If $\Phi\Phi^{\top}$ has repeated monomials at different positions, the corresponding entries of M must coincide. We say "M is consistent".

With these conditions, the cluster moment relaxation of (OT) can be formulated as

$$\inf_{M} \sum_{k \in [K]} \langle C_k, M_k \rangle \tag{OT_{mom}}$$

s.t.
$$M_k^x = \mu\left(\mathbf{R}_x\left(\Phi_k\Phi_k^{\top}\right)\right), \ M_k^y = \nu\left(\mathbf{R}_y\left(\Phi_k\Phi_k^{\top}\right)\right), \ \forall k \in [K]$$
 (5.1a)

$$M_{ij}^{x} := \mu\left(\mathbf{R}_{x}\left(\Phi_{i}\Phi_{j}^{\top}\right)\right), \ M_{ij}^{y} := \nu\left(\mathbf{R}_{y}\left(\Phi_{i}\Phi_{j}^{\top}\right)\right), \ \forall ij \in E(\mathcal{G})$$
 (5.2a)

$$(M_{ij}, M_i, M_j) \in \mathcal{C}_{ij}, \ \forall ij \in [K]_2, \ M \succeq 0 \text{ and consistent},$$
 (5b)

where M is the block moment matrix defined in (32) and the conditions (5.1a)–(5.2a) refer to the OT marginal constraints (28), (29), which stem from the OT marginal constraints (1a) of (OT). Constraints (5b) relax (2.1b)–(2.3b) in (OT_{mar}), reflecting the representability of π_k and π_{ij} as one- and two-marginals of the probability measure π in (1b).

Remark 2.2. When \mathcal{X}_k and \mathcal{Y}_k are semi-algebraic sets defined by polynomial inequalities

$$\mathcal{X}_k = \{x_k : f_{k,l}(x_k) \ge 0, \ l \in [S_k]\}, \qquad \mathcal{Y}_k = \{y_k : g_{k,l}(y_k) \ge 0, \ l \in [S_k]\}, \tag{33}$$

the inequalities can be relaxed into constraints on the moment matrices [36, Sec. 3.2]. Specifically, requiring $q^2 f_{k,l} \geq 0$ (resp. $q^2 g_{k,l}$) for all $q \in \text{span}(\Phi_k)$ such that $q^2 f_{k,l} \in \text{span}(\Phi_k \Phi_k^{\mathsf{T}})$ yields $\mathcal{B}_{k,l}(M_k) \succeq 0$. Here $\mathcal{B}_{k,l}$ is a linear map and the resulting matrix is the *localizing matrix* [31, Sec. 3.2.1], commonly used in polynomial optimization to enforce support constraints. In our marginal relaxation, however, \mathcal{X}_k and \mathcal{Y}_k are discretized, so the support of π_k is handled implicitly. Since the set $\mathcal{X}_k, \mathcal{Y}_k$ are in general not semi-algebraic sets, we do not impose this constraint in (OT_{mom}) .

Problem (OT_{mom}) is a finite-dimensional SDP solvable by standard solvers. However, the presence of multiple PSD blocks in C_{ij} together with the large PSD variable M leads to complicated implementation and high computational cost. Similar to (OT_{mar}¹) and (OT_{mar}²), we therefore consider further relaxations of (OT_{mom}) by dropping either the global or local positivity conditions.

$$\inf_{(M_k, M_{ij})_{[K], E(\mathcal{G})}} \sum_{k \in [K]} \langle C_k, M_k \rangle \tag{OT}_{\text{mom}}^1)$$

s.t.
$$M_k^x = \mu\left(\mathbf{R}_x\left(\Phi_k\Phi_k^{\top}\right)\right), \ M_k^y = \nu\left(\mathbf{R}_y\left(\Phi_k\Phi_k^{\top}\right)\right), \ \forall k \in [K]$$
 (6.1a)

$$M_{ij}^{x} := \mu \left(\mathbf{R}_{x} \left(\Phi_{i} \Phi_{j}^{\top} \right) \right), \ M_{ij}^{y} := \nu \left(\mathbf{R}_{y} \left(\Phi_{i} \Phi_{j}^{\top} \right) \right), \ \forall ij \in E(\mathcal{G})$$
 (6.2a)

$$(M_{ij}, M_i, M_j) \in \mathcal{C}_{ij}$$
 and consistent, $\forall ij \in E(\mathcal{G})$. (6b)

Problem (OT^1_{mom}) is obtained from (OT_{mom}) by dropping the global positivity constraint and removing the variables M_{ij} for $ij \notin E(\mathcal{G})$. It is easier to solve than (OT_{mom}) , as it involves fewer variables and constraints.

$$\inf_{M} \sum_{k \in [K]} \langle C_k, M_k \rangle \tag{OT}_{\text{mom}}^2)$$

s.t.
$$M_k^x = \mu\left(\mathbf{R}_x\left(\Phi_k\Phi_k^{\top}\right)\right), \ M_k^y = \nu\left(\mathbf{R}_y\left(\Phi_k\Phi_k^{\top}\right)\right), \ \forall k \in [K]$$
 (7.1a)

$$M_{ij}^{x} := \mu\left(\mathbf{R}_{x}\left(\Phi_{i}\Phi_{j}^{\top}\right)\right), \ M_{ij}^{y} := \nu\left(\mathbf{R}_{y}\left(\Phi_{i}\Phi_{j}^{\top}\right)\right), \ \forall ij \in E(\mathcal{G})$$
 (7.2a)

$$M \succeq 0$$
 and consistent. (7b)

Problem (OT_{mom}) is obtained from (OT_{mom}) by dropping the local positivity constraints. Remark 2.3. From (25) and (32), the consistency condition (7b) affects only the diagonal blocks M_k 's. Thus, all affine constraints and the objective function involve only the blocks $(M_k, M_{ij})_{[K], E(\mathcal{G})}$. Consequently, as in Remark 2.1, the chordal conversion method of [46] can be applied to exploit the chordal sparsity of \mathcal{G} and decompose (OT_{mom}²) into a multi-block SDP with small matrix variables. For example, when \mathcal{G} is a tree, then problem (OT_{mom}²) can be equivalently reduced into a multi-block SDP problem with variables $(M_k, M_{ij})_{[K], E(\mathcal{G})}$ and local PSD constraints $[M_i, M_{ij}, M_{ij}^{\top}, M_j] \succeq 0$. This can significantly reduce the problem size of (OT_{mom}²).

3 Theoretical analysis of Gaussian distribution

In this section, we analyze the approximation quality of the cluster moment relaxation in the case where both marginals are Gaussian. Let $\mu = \mathcal{N}(m_1, \Sigma_1), \nu = \mathcal{N}(m_2, \Sigma_2)$ with means $m_1, m_2 \in \mathbb{R}^d$ and corvariances $\Sigma_1, \Sigma_2 \in \mathbb{S}^d_{++}$. For the quadratic cost $c(x, y) = ||x - y||^2$, problem (OT) reduces to the squared Wasserstein-2 distance, which admits the closed form

$$W_2^2(\mu,\nu) = \|m_1 - m_2\|^2 + \text{Tr}\Big(\Sigma_1 + \Sigma_2 - 2(\Sigma_1^{1/2}\Sigma_2\Sigma_1^{1/2})^{1/2}\Big).$$
 (34)

Since Gaussians are fully characterized by first and second moments, it suffices to take clusters of single variables and a degree-1 monomial basis $\{1, s\}$. With these choices, the relaxation (OT^2_{mom}) reduces to the SDP

$$\min_{X} \operatorname{Tr}(Z_1) + \operatorname{Tr}(Z_2) - 2\operatorname{Tr}(Y) \tag{35}$$

s.t. $[Z_1]_{\mathcal{G},0} = [\Sigma_1 + m_1 m_1^{\top}]_{\mathcal{G},0}, \quad [Z_2]_{\mathcal{G},0} = [\Sigma_2 + m_2 m_2^{\top}]_{\mathcal{G},0},$

$$X = \begin{bmatrix} 1 & m_1^{\top} & m_2^{\top} \\ m_1 & Z_1 & Y \\ m_2 & Y^{\top} & Z_2 \end{bmatrix} \in \mathbb{S}_+^{2d+1}, \tag{36}$$

where $Z_1, Z_2 \in \mathbb{S}^d, Y \in \mathbb{R}^{d \times d}$ are decision variables. Here, Y represents the cross-covariance between x and y and the operator $[\cdot]_{\mathcal{G},0}$ projects a matrix onto the sparsity pattern \mathcal{G} (Definition D3). Note that, $\Sigma_i + m_i m_i^{\top}$ is simply the second moment matrix of μ or ν .

We now discuss how to reduce the dimension of (35) using chordal conversion. For this, we rely on the following lemma, which is an immediate corollary of the classical results of Grone and Agler [1,19].

Lemma 3.1. Consider the linear SDP

$$\min\left\{\langle A_0, X \rangle : \langle A_i, X \rangle = b_i \ \forall i \in [m], \ X \in \mathbb{S}^n_+\right\},\tag{37}$$

where each $A_i \in \mathbb{S}(G,0)$ for $i \in [m] \sqcup \{0\}$ (Definition D3). If G is chordal with maximal cliques $V_1, \ldots, V_p \subset [n]$, then (37) is equivalent to

$$\min\left\{\langle A_0, X \rangle : \langle A_i, X \rangle = b_i \ \forall i \in [m], \ X \in \mathbb{S}^n(G, 0), \ X_{V_t, V_t} \succeq 0 \ \forall t \in [p]\right\}, \tag{38}$$

which is a multi-block SDP with block sizes $|V_1|, |V_2|, \ldots, |V_p|$.

Using Lemma 3.1, we obtain the following result for (35).

Proposition 3.2. If the reference graph \mathcal{G} (Definition D3) in (35) is chordal with maximal cliques $V_1, \ldots, V_p \subset [d]$, then (35) is equivalent to a multi-block SDP with block sizes $2|V_1| + 1$, $2|V_2| + 1$, ..., $2|V_p| + 1$.

Proof. Define a graph G on vertices [2d+1] whose edges consist of those in the cliques

$$V_i' := \{1\} \sqcup (V_i + 1) \sqcup (V_i + 1 + d), \qquad i \in [p]. \tag{39}$$

This G is precisely the sparsity pattern of (35), and it is chordal with maximal cliques V'_1, \ldots, V'_p . Applying Lemma 3.1 then yields the desired multi-block structure for (35), with block sizes $2|V_i|+1$ for $i \in [p]$.

Remark 3.3. When \mathcal{G} is a tree, its maximal cliques are exactly the edges of \mathcal{G} . In this case, Proposition 3.2 implies that (35) can be reformulated as a multi-block SDP in which each block has size 3. This reduces the SDP dimension from $\mathcal{O}(n^2)$ to $\mathcal{O}(n)$. Moreover, in this setting, (35) coincides with the sparse cluster moment relaxation (OT^1_{mom}) , where the constraint (6b) corresponds to the PSD conditions on these small matrix blocks.

Proposition 3.2 shows how the sparsity of the reference graph \mathcal{G} (Definition D3) can be leveraged to reduce the dimension of the SDP (35). We next establish a result regarding the tightness of our cluster moment relaxation for OT between Gaussian distributions.

Theorem 3.4. Suppose $\Sigma_1, \Sigma_2 \in \mathbb{S}_{++}^d$ satisfy $aI_d \preceq \Sigma_1, \Sigma_2 \preceq bI_d$ for some a, b > 0, and the precision matrices $\Sigma_1^{-1}, \Sigma_2^{-1} \in \mathbb{S}(G,0)$ for a graph $G = ([d], \mathcal{E})$. Let $\operatorname{opt}_{\mathcal{G}}$ denote the optimal value of (35) (special case of $(\operatorname{OT}^2_{\operatorname{mom}})$). We have that:

- (i) If \mathcal{G} is a complete graph, then the relaxation is exact, that is, $\operatorname{opt}_{\mathcal{G}} = W_2^2(\mu, \nu)$.
- (ii) If $\mathcal{G} = G^h$ for some $h \in \mathbb{N}$ (Definition D3), then there exist constants C > 0 and $\rho > 1$, depending only on a, b, such that

$$\left| \operatorname{opt}_{G^h} - W_2^2(\mu, \nu) \right| < C d^{3/2} \rho^{-h}.$$
 (40)

In the above theorem, the assumption Σ_1^{-1} , $\Sigma_2^{-1} \in \mathbb{S}(G,0)$ implies that the two Gaussians are Markovian with respect to the graph G, meaning that variables not connected by an edge in G are conditionally independent given the others. This property, known as *correlative*

sparsity, arises in Gaussian graphical models [52]. The full proof of Theorem 3.4 is given in Appendix A.

Theorem 3.4 (i) establishes the exactness of our cluster moment relaxation (35) (equivalently, (OT_{mom}^2)) for optimal transport between Gaussian distributions when \mathcal{G} is complete. This matches the classical fact that a Gaussian distribution is fully determined by its first and second moments. In practice, these low-order moments can be estimated from a moderate number of samples. In contrast, the standard OT solver that substitutes μ, ν in (OT) with their empirical measures suffers from the curse of dimensionality and requires exponentially many samples in d to achieve comparable accuracy.

Theorem 3.4 (ii) further shows that even in the Gaussian case our convex relaxation improves efficiency. When G is sparse, its neighborhood extensions G^h (Definition D3) also remain sparse for small h, so the relaxation imposes only a limited number of moment constraints. The exponential approximation rate in (40) indicates that a small h already yields an accurate approximation of the true Wasserstein distance. This sparsity enables the use of chordal conversion (see Proposition 3.2) to further reduce the dimension and computational cost of solving the SDP (35).

Although Theorem 3.4 focuses on Gaussian distributions, it helps explain why our convex relaxation reduces both sample and computational complexity. In Section 5, we present numerical evidence showing that our approach also performs well for non-Gaussian distributions. A full theoretical analysis for general distributions is left for future work.

4 Extracting a transport map.

We now explain how to obtain an approximate transport map from the cluster moment relaxation. Consider $\mathcal{X} = \mathcal{Y} = \mathbb{R}^n$ and the quadratic cost $c(x, y) = ||x - y||^2$. The classical dual of (OT) is

$$\sup_{\phi,\psi} \left\{ \int_{\mathcal{X}} \phi(x) \, \mathrm{d}\mu(x) + \int_{\mathcal{Y}} \psi(y) \, \mathrm{d}\nu(y) : \|x - y\|^2 - \phi(x) - \psi(y) \ge 0 \right\}. \tag{41}$$

By Brenier's theorem [7] (see also [51, Theorem 10.28]), if μ and ν are absolutely continuous, the optimal transport plan is induced by a transport map

$$T(x) = x - \frac{1}{2}\nabla\phi(x),\tag{42}$$

where (ϕ, ψ) is the optimal solution of (41). To connect this with our relaxation, recall that (OT^2_{mom}) can be written in standard SDP form as

$$\min_{M} \left\{ \langle C, M \rangle : \ \mathcal{A}^{x}(M) = b^{x}, \ \mathcal{A}^{y}(M) = b^{y}, \ \mathcal{A}^{c}(M) = 0, \ M \succeq 0 \right\}.$$
 (43)

Here, C is block diagonal with $[C]_{k,k} = C_k$ for each $k \in [K]$. The constraints $\mathcal{A}^x(M) = b^x$ and $\mathcal{A}^y(M) = b^y$ represent the affine OT marginal constraints (7.1a) and (7.2a) in the x-and y-coordinates, respectively. Finally, $\mathcal{A}^c(M) = 0$ encodes the consistency constraints, requiring certain groups of entries in M to coincide(recall the definition of consistency in Section 2.3). The dual of (43) is

$$\max_{\lambda} \left\{ \langle b^x, \lambda^x \rangle + \langle b^y, \lambda^y \rangle : C - \mathcal{A}^{x*}(\lambda^x) - \mathcal{A}^{y*}(\lambda^y) - \mathcal{A}^{c*}(\lambda^c) = S, S \succeq 0 \right\}, \tag{44}$$

where $\lambda^x, \lambda^y, \lambda^c$ are the Lagrange multipliers of the affine constraints. We now reformulate (44) as an approximation of the dual formulation (41). Let $\Phi = [\Phi_1; \Phi_2; \dots; \Phi_k]$. From (28), (29), we have

$$b^x = \mu \left(\mathcal{A}^x (\Phi \Phi^\top) \right), \qquad b^y = \nu \left(\mathcal{A}^y (\Phi \Phi^\top) \right).$$
 (45)

Moreover, from (18) and (24), we have that

$$\langle C, \Phi \Phi^{\top} \rangle = \sum_{k \in [K]} \langle C_k, \Phi_k \Phi_k^{\top} \rangle = \sum_{k \in [K]} c_k(z_k) = c(z) = \|x - y\|^2. \tag{46}$$

Finally,

$$\langle \mathcal{A}^{x*}(\lambda^x) + \mathcal{A}^{y*}(\lambda^y) + \mathcal{A}^{c*}(\lambda^c), \Phi \Phi^\top \rangle = \langle \lambda^x, \mathcal{A}^x(\Phi \Phi^\top) \rangle + \langle \lambda^y, \mathcal{A}^y(\Phi \Phi^\top) \rangle, \tag{47}$$

where we used the fact that $\mathcal{A}^{c}(\Phi\Phi^{\top}) = 0$. From (45)–(47), the dual problem (44) can be rewritten as

$$\max_{\lambda} \langle \lambda^{x}, \mu \left(\mathcal{A}^{x}(\Phi \Phi^{\top}) \right) \rangle + \langle \lambda^{y}, \nu \left(\mathcal{A}^{y}(\Phi \Phi^{\top}) \right) \rangle$$
s.t. $\|x - y\|^{2} - \langle \lambda^{x}, \mathcal{A}^{x}(\Phi \Phi^{\top}) \rangle - \langle \lambda^{y}, \mathcal{A}^{y}(\Phi \Phi^{\top}) \rangle = \langle S, \Phi \Phi^{\top} \rangle, \quad S \succeq 0.$ (48)

The term $\{\langle S, \Phi\Phi^{\top} \rangle : S \succeq 0\}$ is precisely the cone of *sum-of-squares (SOS)* polynomials in the basis Φ . Defining $\hat{\phi}(x) := \langle \lambda^x, \mathcal{A}^x(\Phi\Phi^{\top}) \rangle$ and $\hat{\psi}(y) := \langle \lambda^y, \mathcal{A}^y(\Phi\Phi^{\top}) \rangle$, we obtain the equivalent formulation

$$\sup_{\hat{\phi}, \hat{\psi}} \left\{ \int_{\mathcal{X}} \hat{\phi}(x) \, d\mu(x) + \int_{\mathcal{Y}} \hat{\psi}(y) \, d\nu(y) : \|x - y\|^2 - \hat{\phi}(x) - \hat{\psi}(y) \text{ is SOS} \right\}.$$
 (49)

Comparing (41) and (49), we see that the dual SDP is an SOS relaxation of the OT dual: the potentials are restricted to the span of $R_x(\Phi\Phi^{\top})$ and $R_y(\Phi\Phi^{\top})$, and the nonnegativity constraint is replaced by an SOS certificate. From the approximate potential $\hat{\phi}$, we can construct the transport map

$$\widehat{T}(x) = x - \frac{1}{2}\nabla\widehat{\phi}(x),\tag{50}$$

which serves as an approximation of the true map (42).

Although we focus here on the simplified cluster moment relaxation (OT^2_{mom}) , the same procedure applies to the full and sparse versions (OT_{mom}) and (OT^1_{mom}) .

5 Numerical Experiments

In this section, we present numerical experiments to demonstrate the effectiveness of our convex relaxation approaches for high-dimensional OT. We use MOSEK [3] to solve the SDP problems and LP problems. All algorithms are implemented in MATLAB R2024a and executed on a MacBook equipped with an M3 Max chip and 64GB of RAM.

5.1 Gaussian distribution

We first test the cluster moment relaxation for (OT) between Gaussian distributions $\mathcal{N}(m_1, \Sigma_1)$ and $\mathcal{N}(m_2, \Sigma_2)$ to verify Theorem 3.4. The means m_1, m_2 are sampled i.i.d. from a standard normal distribution, and the precision matrices $\Sigma_1^{-1}, \Sigma_2^{-1} \in \mathbb{S}_{++}^d$ are chosen to be sparse, diagonally dominated matrices with a path sparsity pattern G. Off-diagonal entries are drawn i.i.d. from a standard normal distribution, while diagonal entries are set as

$$\Sigma_{1,ii}^{-1} = 0.1 + \sum_{k \neq i} |\Sigma_{1,ik}^{-1}|, \qquad \Sigma_{2,ii}^{-1} = 0.1 + \sum_{k \neq i} |\Sigma_{2,ik}^{-1}|.$$
 (51)

We compute the first and second moments using explicit Gaussian formulas. This is generally infeasible for non-Gaussian distributions, but here we use it solely to verify Theorem 3.4.

We set the reference graph $\mathcal{G} = G^h$ (Definition D3) for $h \in \mathbb{N}^+$ and solve the relaxation (35) with d = 100. The exact value $\operatorname{opt}_{\operatorname{exact}}$ is obtained from (34) and compared with the lower bound $\operatorname{opt}_{\operatorname{SDP}}$, using the relative error

$$\frac{|\text{opt}_{\text{exact}} - \text{opt}_{\text{SDP}}|}{\text{opt}_{\text{exact}}}.$$
 (52)

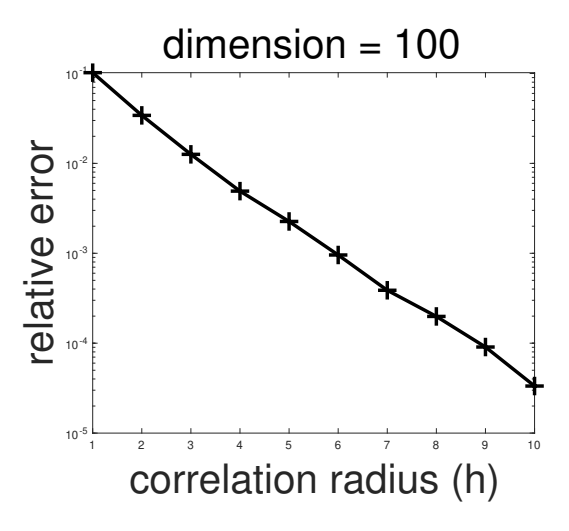


Figure 3: Cluster moment relaxation (35) for OT between Gaussian distributions. The correlation sparsity pattern G of Gaussian distributions is a path. The reference graph \mathcal{G} is chosen as G^h for various correlation radius h (Definition D3).

Figure 3 shows that the cluster moment relaxation exhibits exponential convergence for sparse Gaussian distributions, consistent with (40) in Theorem 3.4.

Next, we compare our cluster moment relaxation with the vanilla OT solver based on sampling approach on the same problem. Specifically, we sample N data points from μ and ν , replace them with their empirical distributions, and solve the resulting discrete OT problem. This leads to an LP with a decision variable of size $N \times N$. For fairness, we also evaluate the moments in our method from the same samples (rather than using Gaussian formulas), and we set the correlation radius h = 5 in the reference graph $\mathcal{G} = G^h$

(Definition D3) of (35). Following Proposition 3.2, we apply chordal conversion to transfer the problem (35) into a multi-block SDP problem with small dimensionality using the MATLAB code SparseCoLO [26].

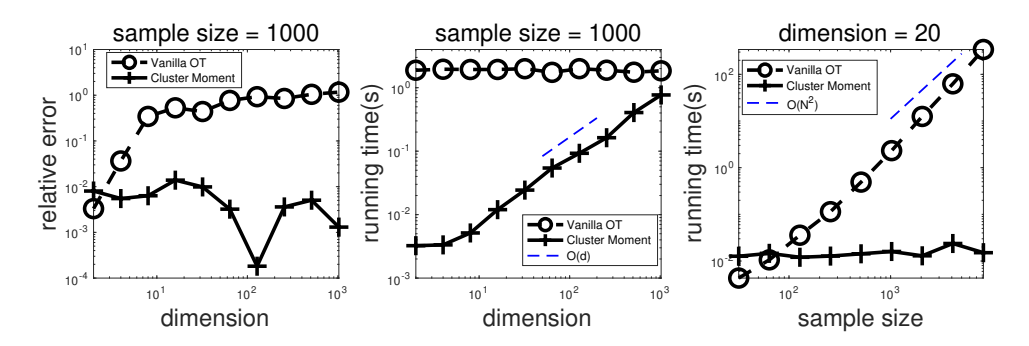


Figure 4: Comparison of cluster moment relaxation (OT_{mom}^2) and the vanilla OT solver for (OT) between Gaussian distributions. The reference graph for (OT_{mom}^2) is $\mathcal{G} = G^h$ (Definition D3), such that G is a path graph and the correlation radius h = 5.

Figure 4 illustrates that the cluster moment relaxation achieves both higher accuracy and greater computational efficiency.

The first panel shows that the relative error of the vanilla OT solver grows rapidly with the problem dimension, whereas that of the cluster moment relaxation remains around or below 10^{-2} . This demonstrates that our method exhibits much smaller sample complexity compared with the vanilla OT solver, which suffers from the curse of dimensionality. The improved performance arises because the cluster moment relaxation relies only on low-order moments of μ and ν , which can be efficiently estimated without requiring large sample sizes.

The second panel reports the running times of solving the SDP problems arising from the cluster moment relaxation and the LP problems from the vanilla OT solver, with tolerance set to 10^{-6} . Although the LP dimension only depends on the sample size (fixed at 1000), the SDP solver consistently runs faster. This is because the chordal conversion substantially reduces the SDP dimension, yielding an overall linear time scaling $\mathcal{O}(d)$.

The third panel shows that solving the SDP associated with the cluster moment relaxation is significantly faster than solving the LP in the vanilla OT formulation. The running time of the vanilla OT solver scales as $\mathcal{O}(N^2)$, while that of the cluster moment relaxation remains essentially constant, $\mathcal{O}(1)$. This is because the vanilla OT formulation involves an LP with $\Omega(N^2)$ variables and $\Omega(N)$ constraints, whereas the SDP (35) has a fixed matrix dimension of 2d+1 and only $\mathcal{O}(hd)$ constraints (linear in d for small h).

5.2 Ising Model

We next test the marginal relaxation for (OT) between Ising models:

$$\mu \sim \exp\left[\beta_1 \left(J_1 \sum_{ij \in E(G)} u_i u_j + h_1 \sum_{k \in [d]} u_k\right)\right],$$

$$\nu \sim \exp\left[\beta_2 \left(J_2 \sum_{ij \in E(G)} v_i v_j + h_2 \sum_{k \in [d]} v_k\right)\right],$$
(53)

where $u_k, v_k \in \{-1, 1\}$ and G is a path graph. For any $\omega \in [d]$, we let $K = \lceil d/\omega \rceil$ and define clusters

$$x_k = \begin{cases} \{u_{(k-1)\omega+1}, \dots, u_{k\omega}\} & k < K \\ \{u_{(k-1)\omega+1}, \dots, u_d\} & k = K \end{cases}$$
 (54)

$$y_k = \begin{cases} \{v_{(k-1)\omega+1}, \dots, v_{k\omega}\} & k < K \\ \{v_{(k-1)\omega+1}, \dots, v_d\} & k = K \end{cases}$$
 (55)

We apply the sparse marginal relaxation (OT_{mar}¹) with the reference graph \mathcal{G} (Definition D3) chosen as a path graph on [K], i.e., edges $\{i(i+1): i \in [K-1]\}$. We set d=12, so that the full density vectors μ, ν (each with 2^{12} entries) can be stored explicitly and the exact OT cost computed. The marginals in (13) are computed exactly from the distributions μ and ν .

Table 1: Marginal relaxation (OT $^1_{mar}$) for (OT) between 1D Ising models. ω is the size of clusters in marginal relaxation defined in (54) and (55). The reference graph $\mathcal G$ (Definition D3) is a path graph.

(J,h,eta)	Method	OT cost	Relative error	time(s)
(1,0.2,0.6)	$\omega = 1$	1.3218923e+01	0	3.90e-03
(-1,0.2,0.6)	$\omega = 2$	1.3218923e+01	0	8.38e-03
	$\omega = 3$	1.3218923e+01	0	7.03e-02
	$\omega = 4$	1.3218923e+01	0	6.09e-01
	exact	1.3218923e+01	0	5.41e + 01
(1,0.2,0.6)	$\omega = 1$	1.9077413e+00	3.20e-1	4.06e-03
(2,0.2,0.44)	$\omega = 2$	2.5413490e+00	9.41e-2	1.05e-02
	$\omega = 3$	2.6937730e+00	3.98e-2	1.01e-01
	$\omega = 4$	2.7297483e+00	2.70e-2	7.59e-01
	exact	2.8054410e+00	0	7.50e + 01
(1,0.2,0.6)	$\omega = 1$	6.5223360e+00	6.20e-2	6.49e-03
(1,0.2,0.2)	$\omega = 2$	6.9073375e+00	6.60e-3	1.02e-02
	$\omega = 3$	6.9073375e+00	6.60e-3	7.95e-02
	$\omega = 4$	6.9443953e+00	1.30e-3	5.61e-01
	exact	6.9535336e+00	0	6.01e+01

Table 1 shows that the lower bound obtained from the marginal relaxation converges to the exact OT cost as ω increases. In the first instance, the relaxation is already tight at $\omega = 1$, demonstrating the effectiveness of the proposed approach even with the smallest clusters. Moreover, the running time for solving the LP arising from the marginal relaxation is several orders of magnitude smaller than that of the original problem (OT). This improvement stems from the fact that our marginal relaxation substantially reduces the number of variables and constraints in the LP formulation.

Next, we compare our marginal relaxation with the vanilla OT solver. Since the exact ground truth cannot be obtained by directly solving (OT) in high-dimensional settings, we construct a case where the true OT cost is known. Specifically, we set $(J_1, h_1, \beta_1) = (J_2, h_2, \beta_2) = (-1, 0.2, 0.3)$ so that the exact OT cost equals zero. We then generate N samples from μ and ν using tensor train conditional sampling [14, 41] and estimate their marginals from these samples for use in the marginal relaxation (OT¹_{mar}). We choose $\omega = 1$, which is already exact when $\mu = \nu$. For the standard OT solver, we discretize the problem into an $N \times N$ formulation, following the same procedure as in the Gaussian case described in Subsection 5.1.

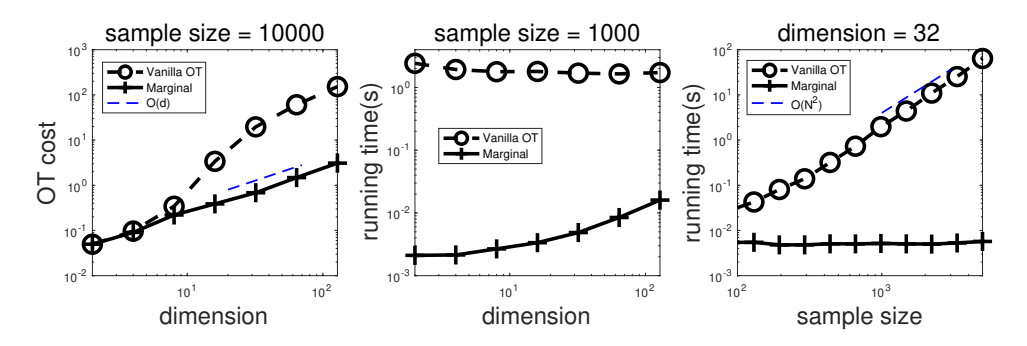


Figure 5: Comparison of marginal relaxation and traditional OT solver for (OT) between Ising models with $(J_1, h_1, \beta_1) = (J_2, h_2, \beta_2) = (-1, 0.2, 0.3)$. $\omega = 1$ is the size of clusters in marginal relaxation defined in (54) and (55).

The first panel in Figure 5 shows that the OT cost obtained from the marginal relaxation remains consistently closer to zero (the ground truth) than that from the vanilla OT solver across all dimensions. In addition, the OT cost of marginal relaxation scales like a linear function of the dimension while that of vanilla OT solver blow up quickly. This indicates that the marginal relaxation substantially reduces the sample complexity. This is because it depends only on marginal distributions, which can be estimated with far fewer samples than the full OT formulation.

The second panel of Figure 5 reports the running times for the LPs arising from our marginal relaxation and from the vanilla OT solver. As in the Gaussian case, the LP dimension in the vanilla solver depends only on the sample size (fixed at 1000). Nonetheless, our marginal relaxation remains significantly faster because the small cluster size ω yields LPs of much lower dimensionality.

The third panel in Figure 5 highlights the dramatic difference in computational cost: solving the LPs in the marginal relaxation takes less than a second, whereas the vanilla OT solver must handle large-scale LP problems and is significantly slower. These results

underscore the practical advantages of the marginal relaxation over vanilla OT solver.

5.3 Ginzburg-Landau Model

Finally, we test our cluster moment relaxation for generative modeling task from 1D Ginzburg–Landau model:

$$\nu \sim \exp\left[-\beta \left(\sum_{i=1}^{d+1} \frac{\lambda}{2} \left(\frac{y_i - y_{i-1}}{h}\right)^2 + \frac{1}{4\lambda} (1 - y_i^2)^2\right)\right], \quad y \in [-L, L]^d, \tag{56}$$

with boundary conditions $x_0 = x_{d+1} = y_0 = y_{d+1} = 0$, step size h = 1/(1+d) and L = 2.5.

In order to use our cluster moment relaxation in general modeling task, we first generate $N=10^4$ training samples from ν using tensor-train conditional sampling [14,41]. We compute the mean m and corvariance Σ from these samples and use them to form a Gaussian distribution $\mu \sim \mathcal{N}(m, \Sigma)$. We then generate another $N=10^4$ sample points from μ and use these samples from μ and ν to train our transport map \widehat{T} (50) using the procedure in Section 4. The moments of μ and ν are estimated from these samples and imposed as marginal constraints in the cluster moment relaxation $(\mathrm{OT}^2_{\mathrm{mom}})$ with K=d and the reference graph \mathcal{G} (Definition D3) being a path graph. We use the monomial basis Φ_k consisting of all monomials of degree at most n=10 within cluster z_k . Following Remark 2.3, we apply chordal conversion to reformulate $(\mathrm{OT}^2_{\mathrm{mom}})$ as a multi-block SDP with small block sizes, using the MATLAB package SparseCoLO [26].

After extracting the transport map \widehat{T} (50) from the SDP solution. We apply it to another 10^5 reference samples from μ . The quality of \widehat{T} is assessed by comparing the pairwise marginals of the mapped samples with those of an independent reference set of 10^5 samples from ν .

We also compare our approach with a neural network method using normalizing flows [37]. The neural network is trained on the same training data. Note that the transport map generated from normalizing flow does not generally yield the Monge optimal transport map; our aim here is solely to compare accuracy. Following [41], the normalizing flow model uses five transforms, each implemented as a three-layer neural network with width 128.

We first test a 10-dimensional instance with parameters $\beta=1/8$, L=2.5, and $\lambda=0.03$. As shown in Figure 6, both the cluster moment relaxation and the neural network method capture the support of the pairwise marginals of ν . However, the convex relaxation yields noticeably higher accuracy than the neural network approach. We next test a 50-dimensional instance with parameters $\beta=1/20$, L=2.5, and $\lambda=0.01$. Figure 7 shows that the cluster moment relaxation achieves substantially better accuracy than the transport map produced by the neural network method. These results demonstrate the effectiveness of the proposed cluster moment relaxation for generative modeling.

6 Conclusion

In this paper, we proposed convex relaxation approaches for addressing the high dimensionality of optimal transport. By introducing marginal and cluster moment relaxations, we obtain tractable convex programs that provide computable lower bounds and enable

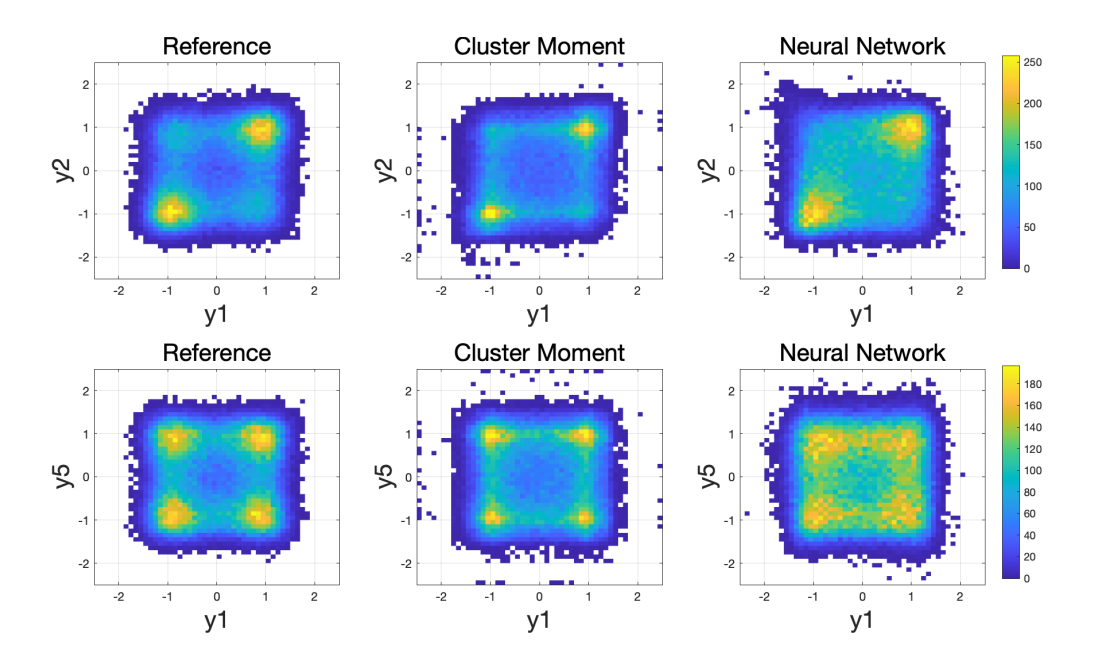


Figure 6: Comparison of the cluster moment relaxation (OT_{mom}^2) and a neural network method for generative modeling of the 1D Ginzburg–Landau model (d=10, $\beta=1/8$, L=2.5, $\lambda=0.03$). For the cluster moment relaxation, we set the number of clusters K=10 and relaxation degree n=10, and use a path graph as the reference graph \mathcal{G} (Definition D3). The first and fourth panels show the empirical marginals of reference samples from μ , while the remaining panels display the corresponding marginals after applying the transport maps obtained by the two methods.

the extraction of transport maps. Our theoretical analysis in the Gaussian setting shows exponential convergence under correlative sparsity, and numerical experiments demonstrate that the approach extends effectively to non-Gaussian distributions. Furthermore, we illustrated the potential of transport maps derived from these relaxations as alternatives to neural networks in generative modeling. These results highlight convex relaxation as a promising dimension reduction framework for scaling OT to high-dimensional problems.

A Proof details

In this section, we state the proof of Theorem 3.4. Throughout this section, we always assume that μ , ν are Gaussian distributions $\mathcal{N}(m_1, \Sigma_1), \mathcal{N}(m_2, \Sigma_2)$ for some $\Sigma_1, \Sigma_2 \succ 0$. In order to proof Theorem 3.4, we need the following lemma, which provides an error bound between the convex relaxation (35) and the exact OT cost (34).

Lemma A.1. Suppose the optimal value of (35) is $opt_{\mathcal{G}}$, then

$$W_2^2(\mu,\nu) - \epsilon_{\mathcal{G}} \le \text{opt}_{\mathcal{G}} \le W_2^2(\mu,\nu), \tag{57}$$

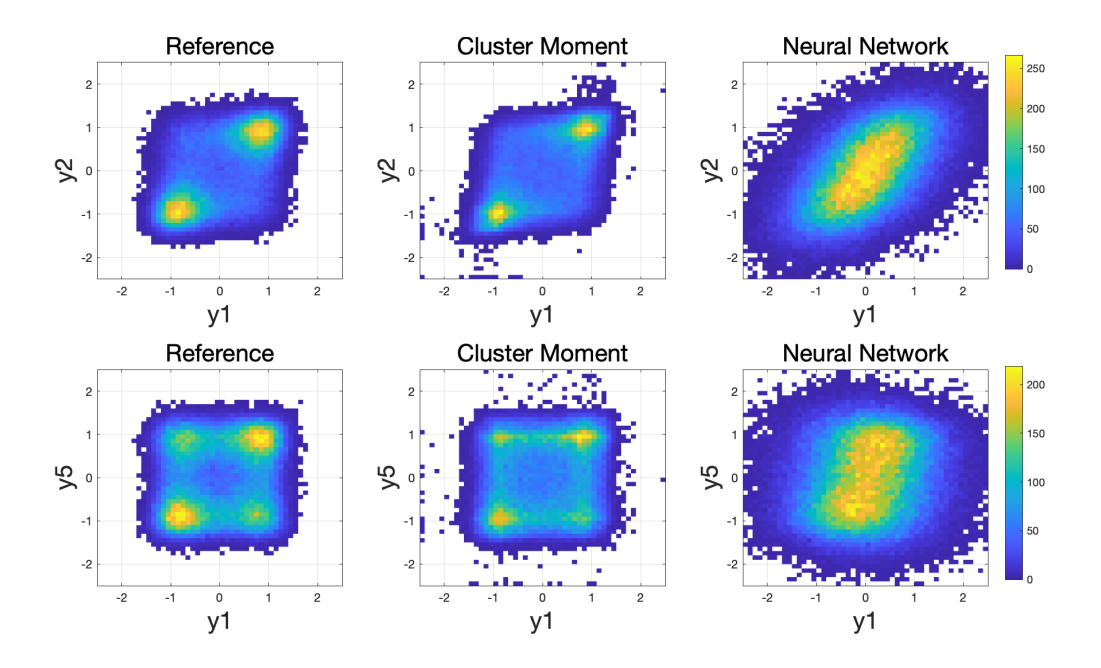


Figure 7: Comparison of the cluster moment relaxation (OT^2_{mom}) and a neural network method for generative modeling of the 1D Ginzburg–Landau model ($d=50,\,\beta=1/20,\,L=2.5,\,\lambda=0.01$). For the cluster moment relaxation, we set the number of clusters K=50 and relaxation degree n=10, and use a path graph as the reference graph $\mathcal G$ (Definition D3). The first and fourth panels show the empirical marginals of reference samples from μ , while the remaining panels display the corresponding marginals after applying the transport maps obtained by the two methods.

where

$$\epsilon_{\mathcal{G}} := 2 \operatorname{Tr}(\Sigma_{1}) \left\| \left[\Sigma_{1}^{-1/2} \left[\Sigma_{1}^{1/2} \Sigma_{2} \Sigma_{1}^{1/2} \right]^{1/2} \Sigma_{1}^{-1/2} \right]_{\mathcal{G}, c} \right\|_{2} + 2 \operatorname{Tr}(\Sigma_{2}) \left\| \left[\Sigma_{1}^{1/2} \left[\Sigma_{1}^{1/2} \Sigma_{2} \Sigma_{1}^{1/2} \right]^{-1/2} \Sigma_{1}^{1/2} \right]_{\mathcal{G}, c} \right\|_{2}.$$

$$(58)$$

The operator $[\cdot]_{\mathcal{G},c}$ projects a matrix onto the complement of the sparsity pattern \mathcal{G} (Definition D3).

Proof. The problem (35) can be simplified into the following problem by using the Schur complement of the first entry of X as the decision variable

min
$$||m_1 - m_2||^2 + \text{Tr}(\Sigma_1) + \text{Tr}(\Sigma_2) - 2\text{Tr}(Y)$$

s.t. $[Z_1]_{\mathcal{G}} = [\Sigma_1]_{\mathcal{G}}, \quad [Z_2]_{\mathcal{G}} = [\Sigma_2]_{\mathcal{G}},$

$$\begin{bmatrix} Z_1 & Y \\ Y^\top & Z_2 \end{bmatrix} \in \mathbb{S}_+^{2d},$$
(59)

where the operator $[\cdot]_{\mathcal{G}}$ projects a matrix onto the sparsity pattern \mathcal{G} (Definition D3). The

dual problem of (59) is:

$$\max \|m_1 - m_2\|^2 + \operatorname{Tr}(\Sigma_1) + \operatorname{Tr}(\Sigma_2) - \langle \Sigma_1, \Lambda_1 \rangle - \langle \Sigma_2, \Lambda_2 \rangle$$
s.t.
$$\begin{bmatrix} \Lambda_1 & -I_d \\ -I_d & \Lambda_2 \end{bmatrix} \in \mathbb{S}_+^{2d}, \ \Lambda_1, \Lambda_2 \in \mathbb{S}^d(\mathcal{G}, 0),$$
(60)

where $\mathbb{S}^d(\mathcal{G},0)$ is defined in (6). When \mathcal{G} is complete graph, (59) and (60) become

$$\min \left\{ \|m_1 - m_2\|^2 + \operatorname{Tr}(\Sigma_1) + \operatorname{Tr}(\Sigma_2) - 2\operatorname{Tr}(Y) : \begin{bmatrix} \Sigma_1 & Y \\ Y^\top & \Sigma_2 \end{bmatrix} \in \mathbb{S}_+^{2d} \right\}, \tag{61}$$

and

$$\max \left\{ \|m_1 - m_2\|^2 + \operatorname{Tr}(\Sigma_1) + \operatorname{Tr}(\Sigma_2) - \langle \Sigma_1, \Lambda_1 \rangle - \langle \Sigma_2, \Lambda_2 \rangle : \begin{bmatrix} \Lambda_1 & -I_d \\ -I_d & \Lambda_2 \end{bmatrix} \in \mathbb{S}_+^{2d} \right\}, \quad (62)$$

respectively. The problem (61) and (62) have the following closed form solutions, whose function values are exactly $W_2^2(\mu,\nu)$.

$$\begin{bmatrix} \Sigma_1 & \Sigma_1^{1/2} \left[\Sigma_1^{1/2} \Sigma_2 \Sigma_1^{1/2} \right]^{1/2} \Sigma_1^{-1/2} \\ \Sigma_1^{-1/2} \left[\Sigma_1^{1/2} \Sigma_2 \Sigma_1^{1/2} \right]^{1/2} \Sigma_1^{1/2} & \Sigma_2 \end{bmatrix}, \tag{63}$$

$$\begin{bmatrix} \Sigma_{1}^{-1/2} \left[\Sigma_{1}^{1/2} \Sigma_{2} \Sigma_{1}^{1/2} \right]^{1/2} \Sigma_{1}^{-1/2} & -I_{d} \\ -I_{d} & \Sigma_{1}^{1/2} \left[\Sigma_{1}^{1/2} \Sigma_{2} \Sigma_{1}^{1/2} \right]^{-1/2} \Sigma_{1}^{1/2} \end{bmatrix}.$$
(64)

One can easily check that (63) and (64) satisfy the constraints in (61) and (62), with objective values equal to the exact OT cost (34). Let

$$\widehat{\Lambda}_1 := \Sigma_1^{-1/2} \left[\Sigma_1^{1/2} \Sigma_2 \Sigma_1^{1/2} \right]^{1/2} \Sigma_1^{-1/2}, \quad \widehat{\Lambda}_2 := \Sigma_1^{1/2} \left[\Sigma_1^{1/2} \Sigma_2 \Sigma_1^{1/2} \right]^{-1/2} \Sigma_1^{1/2}$$
 (65)

be the diagonal blocks of the matrix in (64).

Now, we come back to the problems (59) and (60), where \mathcal{G} may not be a complete graph. Although they may not have close form solutions, we can modify $\widehat{\Lambda}_1, \widehat{\Lambda}_2$ to get feasible dual solutions (need not be optimal) of (60). In detail, we set the entries of $\widehat{\Lambda}_1, \widehat{\Lambda}_2$ outside the sparsity pattern \mathcal{G} to be zero and then add constant identity matrices to preserve the PSD condition. As a result, we obtain the following feasible solutions of (60):

$$\widetilde{\Lambda}_1 = \widehat{\Lambda}_1 - [\widehat{\Lambda}_1]_{\mathcal{G},c} + \|[\widehat{\Lambda}_1]_{\mathcal{G},c}\|_2 I_d, \quad \widetilde{\Lambda}_2 = \widehat{\Lambda}_2 - [\widehat{\Lambda}_2]_{\mathcal{G},c} + \|[\widehat{\Lambda}_2]_{\mathcal{G},c}\|_2 I_d.$$
 (66)

Substituting (66) into (60), we get

$$||m_{1} - m_{2}||^{2} + \operatorname{Tr}(\Sigma_{1}) + \operatorname{Tr}(\Sigma_{2}) - \left\langle \Sigma_{1}, \widetilde{\Lambda}_{1} \right\rangle - \left\langle \Sigma_{2}, \widetilde{\Lambda}_{2} \right\rangle$$

$$= ||m_{1} - m_{2}||^{2} + \operatorname{Tr}(\Sigma_{1}) + \operatorname{Tr}(\Sigma_{2}) - \left\langle \Sigma_{1}, \widehat{\Lambda}_{1} \right\rangle - \left\langle \Sigma_{2}, \widehat{\Lambda}_{2} \right\rangle$$

$$- \left\langle \Sigma_{1}, -[\widehat{\Lambda}_{1}]_{\mathcal{G},c} + ||[\widehat{\Lambda}_{1}]_{\mathcal{G},c}||_{2}I_{d} \right\rangle - \left\langle \Sigma_{2}, -[\widehat{\Lambda}_{2}]_{\mathcal{G},c} + ||[\widehat{\Lambda}_{2}]_{\mathcal{G},c}||_{2}I_{d} \right\rangle$$

$$\geq W_{2}^{2}(\mu, \nu) - \left\langle \Sigma_{1}, 2||[\widehat{\Lambda}_{1}]_{\mathcal{G},c}||_{2}I_{d} \right\rangle - \left\langle \Sigma_{2}, 2||[\widehat{\Lambda}_{2}]_{\mathcal{G},c}||_{2}I_{d} \right\rangle, \tag{67}$$

where the inequality comes from the optimality of $(\widehat{\Lambda}_1, \widehat{\Lambda}_2)$ for (60), whose optimal value is $W_2^2(\mu, \nu)$ and the PSD of matrices Σ_1, Σ_2 . The inequality (67) implies left hand side inequality of (57). As for the right hand side, it is immediate because the cluster moment relaxation provides a lower bound of the exact OT cost.

With this lemma, we are now able to prove Theorem 3.4.

Proof of Theorem 3.4

Proof. When \mathcal{G} is a complete graph, from (58) in Lemma A.1, we have that $\epsilon_{\mathcal{G}} = 0$. Thus, (57) implies the relaxation is exact. This completes the proof of (i) in Theorem 3.4.

When $\mathcal{G} = G^h$ for some $h \in \mathbb{N}$, from Lemma A.1, we only have to show that ϵ_{G^h} in (58) satisfies the inequality (40) in Theorem 3.4. Our proof idea is motivated from the Demko-Moss-Smith theorem [13]. Because $bI_d \succeq \Sigma_1, \Sigma_2 \succeq aI_d$, we have that

$$a^{-2}I_d \succeq \Sigma_1^{-1/2} \Sigma_2^{-1} \Sigma_1^{-1/2} \succeq b^{-2}I_d. \tag{68}$$

From approximation theorem of Chebyshev polynomials [48], we have that there exists $C_{a,b} > 0$ such that for any $k \in \mathbb{N}^+$, there a degree k polynomial p_k such that

$$||x^{-1/2} - p_k(x)||_{\infty, [b^{-2}, a^{-2}]} \le C_{a,b} \rho_{a,b}^{-k}$$
(69)

where $C_{a,b} > 0, \rho_{a,b} > 1$ are parameters that only depend on a and b. From (69), we have that

$$\left\| \left[\Sigma_1^{1/2} \Sigma_2 \Sigma_1^{1/2} \right]^{1/2} - p_k \left(\Sigma_1^{-1/2} \Sigma_2^{-1} \Sigma_1^{-1/2} \right) \right\|_2 \le C_{a,b} \rho_{a,b}^{-k}.$$
 (70)

From (70), we have that for any $h \in \mathbb{N}^+$,

$$\left\| \left[\Sigma_{1}^{-1/2} \left[\Sigma_{1}^{1/2} \Sigma_{2} \Sigma_{1}^{1/2} \right]^{1/2} \Sigma_{1}^{-1/2} \right]_{G^{h},c} \right\|_{2} \\
\leq \left\| \left[\Sigma_{1}^{-1/2} p_{k} \left(\Sigma_{1}^{-1/2} \Sigma_{2}^{-1} \Sigma_{1}^{-1/2} \right) \Sigma_{1}^{-1/2} \right]_{G^{h},c} \right\|_{2} \\
+ \left\| \Sigma_{1}^{-1/2} \left[\left[\Sigma_{1}^{1/2} \Sigma_{2} \Sigma_{1}^{1/2} \right]^{1/2} - p_{k} \left(\Sigma_{1}^{-1/2} \Sigma_{2}^{-1} \Sigma_{1}^{-1/2} \right) \right] \Sigma_{1}^{-1/2} \right\|_{F} \\
\leq \left\| \left[\Sigma_{1}^{-1/2} p_{k} \left(\Sigma_{1}^{-1/2} \Sigma_{2}^{-1} \Sigma_{1}^{-1/2} \right) \Sigma_{1}^{-1/2} \right]_{G^{h},c} \right\|_{2} + C_{a,b} a^{-1} d^{1/2} \rho_{a,b}^{-k}. \tag{71}$$

Because p_k is a degree k polynomial, let it be $\sum_{i=0}^k \gamma_i x^i$. Then we have that

$$\Sigma_{1}^{-1/2} p_{k} \left(\Sigma_{1}^{-1/2} \Sigma_{2}^{-1} \Sigma_{1}^{-1/2} \right) \Sigma_{1}^{-1/2} = \sum_{i=0}^{k} \gamma_{i} \Sigma_{1}^{-1/2} \left(\Sigma_{1}^{-1/2} \Sigma_{2}^{-1} \Sigma_{1}^{-1/2} \right)^{i} \Sigma_{1}^{-1/2}
= \sum_{i=0}^{k} \gamma_{i} \left(\Sigma_{1}^{-1} \Sigma_{2}^{-1} \right)^{i} \Sigma_{1}^{-1} = p_{k} \left(\Sigma_{1}^{-1} \Sigma_{2}^{-1} \right) \Sigma_{1}^{-1}.$$
(72)

Because Σ_1^{-1} , $\Sigma_2^{-1} \in \mathbb{S}(G,0)$ and we have that when $h \geq 2k+1$, $[p_k(\Sigma_1^{-1}\Sigma_2^{-1})\Sigma_1^{-1}]_{G^h,c} = 0$. Substituting this into (71), we get for any $h \geq 2k+1$,

$$\left\| \left[\Sigma_1^{-1/2} \left[\Sigma_1^{1/2} \Sigma_2 \Sigma_1^{1/2} \right]^{1/2} \Sigma_1^{-1/2} \right]_{G^h, c} \right\|_2 \le C_{a,b} a^{-1} d^{1/2} \rho_{a,b}^{-k}. \tag{73}$$

From (70), for any $h \in \mathbb{N}^+$

$$\begin{split}
& \left\| \left[\Sigma_{1}^{1/2} \left[\Sigma_{1}^{1/2} \Sigma_{2} \Sigma_{1}^{1/2} \right]^{-1/2} \Sigma_{1}^{1/2} \right]_{G^{h}, c} \right\|_{2} \\
&= \left\| \left[\Sigma_{1}^{1/2} \left[\Sigma_{1}^{1/2} \Sigma_{2} \Sigma_{1}^{1/2} \right]^{-1} \left[\Sigma_{1}^{1/2} \Sigma_{2} \Sigma_{1}^{1/2} \right]^{1/2} \Sigma_{1}^{1/2} \right]_{G^{h}, c} \right\|_{2} \\
&= \left\| \left[\Sigma_{2}^{-1} \Sigma_{1}^{-1/2} \left[\Sigma_{1}^{1/2} \Sigma_{2} \Sigma_{1}^{1/2} \right]^{1/2} \Sigma_{1}^{1/2} \right]_{G^{h}, c} \right\|_{2} \\
&\leq \left\| \left[\Sigma_{2}^{-1} \Sigma_{1}^{-1/2} p_{k} \left(\Sigma_{1}^{-1/2} \Sigma_{2}^{-1} \Sigma_{1}^{-1/2} \right) \Sigma_{1}^{1/2} \right]_{G^{h}, c} \right\|_{2} \\
&+ \left\| \Sigma_{2}^{-1} \Sigma_{1}^{-1/2} \left[\left[\Sigma_{1}^{1/2} \Sigma_{2} \Sigma_{1}^{1/2} \right]^{1/2} - p_{k} \left(\Sigma_{1}^{-1/2} \Sigma_{2}^{-1} \Sigma_{1}^{-1/2} \right) \right] \Sigma_{1}^{1/2} \right\|_{F} \\
&\leq \left\| \left[\Sigma_{2}^{-1} \Sigma_{1}^{-1/2} p_{k} \left(\Sigma_{1}^{-1/2} \Sigma_{2}^{-1} \Sigma_{1}^{-1/2} \right) \Sigma_{1}^{1/2} \right]_{G^{h}, c} \right\|_{2} + C_{a, b} b^{1/2} a^{-3/2} d^{1/2} \rho_{a, b}^{-k}. \tag{74}
\end{split}$$

Similar to (72), we have that $\Sigma_2^{-1}\Sigma_1^{-1/2}p_k\left(\Sigma_1^{-1/2}\Sigma_2^{-1}\Sigma_1^{-1/2}\right)\Sigma_1^{1/2} = \Sigma_2^{-1}p_k\left(\Sigma_1^{-1}\Sigma_2^{-1}\right)$, which implies that $\left[\Sigma_2^{-1}\Sigma_1^{-1/2}p_k\left(\Sigma_1^{-1/2}\Sigma_2^{-1}\Sigma_1^{-1/2}\right)\Sigma_1^{1/2}\right]_{G^h,c} = 0$ for any $h \ge 2k + 1$. Substituting this into (74), we have that for any $h \ge 2k + 1$,

$$\left\| \left[\Sigma_1^{1/2} \left[\Sigma_1^{1/2} \Sigma_2 \Sigma_1^{1/2} \right]^{-1/2} \Sigma_1^{1/2} \right]_{G^h, c} \right\|_2 \le C_{a,b} b^{1/2} a^{-3/2} d^{1/2} \rho_{a,b}^{-k}. \tag{75}$$

Substituting (73), (75) into (58), we have that for any $h \ge 2k + 1$,

$$\epsilon_{G^h} \le 2\text{Tr}(\Sigma_1) C_{a,b} a^{-1} d^{1/2} \rho_{a,b}^{-k} + 2\text{Tr}(\Sigma_2) C_{a,b} b^{1/2} a^{-3/2} d^{1/2} \rho_{a,b}^{-k}.$$
 (76)

Because $\text{Tr}(\Sigma_1), \text{Tr}(\Sigma_2) \leq bd$, we have that

$$\epsilon_{G^h} \le 2 \left(C_{a,b} a^{-3/2} b^{3/2} + C_{a,b} a^{-1} b \right) d^{3/2} \rho_{a,b}^{-k}.$$
 (77)

Since the above inequality holds for all $h, k \in \mathbb{N}^+$ such that $h \geq 2k + 1$, we have that for any $h \geq 3$,

$$\epsilon_{G^h} \le 2 \left(C_{a,b} a^{-3/2} b^{3/2} + C_{a,b} a^{-1} b \right) d^{3/2} \rho_{a,b}^{-(h-2)/2}.$$
(78)

which can be rewritten as

$$\epsilon_{G^h} \le C'_{a,b} d^{3/2} \left[\rho_{a,b}^{-1/2} \right]^h, \ \forall h \ge 3.$$
 (79)

where $C'_{a,b} > 0$ only depends on a, b. Because the bound (79) only holds for $h \ge 3$, we have to extend it to all $h \in \mathbb{N}$. Note that from (58), we have that the following naive bound holds

$$\epsilon_{Gh} \le 4b^2 a^{-1} d^{3/2}, \ \forall h \in \mathbb{N}. \tag{80}$$

Combining (79) and (81), we get that

$$\epsilon_{G^h} \le \left(C'_{a,b} + 4b^2 a^{-1} \rho_{a,b}^2 \right) d^{3/2} \cdot \left[\rho_{a,b}^{-1/2} \right]^h, \ \forall h \in \mathbb{N}.$$
(81)

This completes the proof of (ii) in Theorem 3.4.

Acknowledgments.

The authors thank Siyao Yang for assistance with the sampling procedures and Yifan Peng for providing the neural network code used in our numerical experiments. In particular, the first author, Yuehaw Khoo, would like to thank Gero Friesecke for their valuable discussions on high-dimensional optimal transport.

References

- [1] J. Agler, W. Helton, S. McCullough, and L. Rodman. Positive semidefinite matrices with a given sparsity pattern. *Linear algebra and its applications*, 107:101–149, 1988.
- [2] G. An. A note on the cluster variation method. *Journal of Statistical Physics*, 52(3):727–734, 1988.
- [3] M. Aps. Mosek optimization toolbox for matlab. *User's Guide and Reference Manual Version*, 4(1):116, 2019.
- [4] M. Arjovsky, S. Chintala, and L. Bottou. Wasserstein generative adversarial networks. In *International conference on machine learning*, pages 214–223. PMLR, 2017.
- [5] Y. Balaji, R. Chellappa, and S. Feizi. Robust optimal transport with applications in generative modeling and domain adaptation. *Advances in Neural Information Processing Systems*, 33:12934–12944, 2020.
- [6] N. Bonneel, J. Rabin, G. Peyré, and H. Pfister. Sliced and radon wasserstein barycenters of measures. *Journal of Mathematical Imaging and Vision*, 51(1):22–45, 2015.
- [7] Y. Brenier. Polar factorization and monotone rearrangement of vector-valued functions. Communications on pure and applied mathematics, 44(4):375–417, 1991.
- [8] J. Calder and N. G. Trillos. Improved spectral convergence rates for graph laplacians on ε -graphs and k-nn graphs. Applied and Computational Harmonic Analysis, 60:123–175, 2022.

- [9] Y. Chen, Y. Khoo, and L.-H. Lim. Convex relaxation for fokker-planck equation. In *Proceedings A*, volume 481, page 20240001. The Royal Society, 2025.
- [10] Y. Chen, Y. Khoo, and M. Lindsey. Multiscale semidefinite programming approach to positioning problems with pairwise structure. *Journal of Scientific Computing*, 101(2):42, 2024.
- [11] X. Cheng, J. Lu, Y. Tan, and Y. Xie. Convergence of flow-based generative models via proximal gradient descent in wasserstein space. *IEEE Transactions on Information Theory*, 70(11):8087–8106, 2024.
- [12] A. Cloninger, K. Hamm, V. Khurana, and C. Moosmüller. Linearized wasserstein dimensionality reduction with approximation guarantees. Applied and Computational Harmonic Analysis, 74:101718, 2025.
- [13] S. Demko, W. F. Moss, and P. W. Smith. Decay rates for inverses of band matrices. *Mathematics of computation*, 43(168):491–499, 1984.
- [14] S. Dolgov, K. Anaya-Izquierdo, C. Fox, and R. Scheichl. Approximation and sampling of multivariate probability distributions in the tensor train decomposition. *Statistics* and Computing, 30(3):603–625, 2020.
- [15] R. M. Dudley. The speed of mean glivenko-cantelli convergence. The Annals of Mathematical Statistics, 40(1):40–50, 1969.
- [16] N. Fournier and A. Guillin. On the rate of convergence in wasserstein distance of the empirical measure. Probability theory and related fields, 162(3):707-738, 2015.
- [17] G. Friesecke. Optimal Transport: A Comprehensive Introduction to Modeling, Analysis, Simulation, Applications. SIAM, 2024.
- [18] A. Genevay, G. Peyré, and M. Cuturi. Learning generative models with sinkhorn divergences. In *International Conference on Artificial Intelligence and Statistics*, pages 1608–1617. PMLR, 2018.
- [19] R. Grone, C. R. Johnson, E. M. Sá, and H. Wolkowicz. Positive definite completions of partial Hermitian matrices. *Linear algebra and its applications*, 58:109–124, 1984.
- [20] D. Hou, T. Tang, and K.-C. Toh. A low-rank augmented lagrangian method for doubly nonnegative relaxations of mixed-binary quadratic programs. *Operations Research*, 2025.
- [21] D. Hou, T. Tang, and K.-C. Toh. Rinnal+: a riemannian alm solver for sdp-rlt relaxations of mixed-binary quadratic programs. arXiv preprint arXiv:2507.13776, 2025.
- [22] J.-C. Hütter and P. Rigollet. Minimax estimation of smooth optimal transport maps. The Annals of Statistics, 49(2), 2021.

- [23] L. V. Kantorovich. On the translocation of masses. In Dokl. Akad. Nauk. USSR (NS), volume 37, pages 199–201, 1942.
- [24] Y. Khoo, L. Lin, M. Lindsey, and L. Ying. Semidefinite relaxation of multimarginal optimal transport for strictly correlated electrons in second quantization. SIAM Journal on Scientific Computing, 42(6):B1462–B1489, 2020.
- [25] Y. Khoo and L. Ying. Convex relaxation approaches for strictly correlated density functional theory. SIAM Journal on Scientific Computing, 41(4):B773–B795, 2019.
- [26] S. Kim, M. Kojima, M. Mevissen, and M. Yamashita. Exploiting sparsity in linear and nonlinear matrix inequalities via positive semidefinite matrix completion. *Mathematical* programming, 129(1):33–68, 2011.
- [27] A. Korotin, D. Selikhanovych, and E. Burnaev. Neural optimal transport. arXiv preprint arXiv:2201.12220, 2022.
- [28] S. Kullback and R. A. Leibler. On information and sufficiency. The Annals of Mathematical Statistics, 22(1):79–86, 1951.
- [29] J. B. Lasserre. Global optimization with polynomials and the problem of moments. SIAM Journal on optimization, 11(3):796–817, 2001.
- [30] J. B. Lasserre. A semidefinite programming approach to the generalized problem of moments. *Mathematical Programming*, 112(1):65–92, 2008.
- [31] J. B. Lasserre. Moments, positive polynomials and their applications, volume 1. World Scientific, 2009.
- [32] T. Lin, C. Fan, N. Ho, M. Cuturi, and M. Jordan. Projection robust wasserstein distance and riemannian optimization. Advances in neural information processing systems, 33:9383–9397, 2020.
- [33] A. Makkuva, A. Taghvaei, S. Oh, and J. Lee. Optimal transport mapping via input convex neural networks. In *International Conference on Machine Learning*, pages 6672–6681. PMLR, 2020.
- [34] P. Mokrov, A. Korotin, L. Li, A. Genevay, J. M. Solomon, and E. Burnaev. Large-scale wasserstein gradient flows. Advances in Neural Information Processing Systems, 34:15243–15256, 2021.
- [35] G. Monge. Mémoire sur la théorie des déblais et des remblais. Mem. Math. Phys. Acad. Royale Sci., pages 666-704, 1781.
- [36] O. Mula and A. Nouy. Moment-sos methods for optimal transport problems. *Numerische Mathematik*, 156(4):1541–1578, 2024.
- [37] G. Papamakarios, T. Pavlakou, and I. Murray. Masked autoregressive flow for density estimation. Advances in neural information processing systems, 30, 2017.

- [38] F.-P. Paty and M. Cuturi. Subspace robust wasserstein distances. In *International conference on machine learning*, pages 5072–5081. PMLR, 2019.
- [39] A. Pelizzola. Cluster variation method in statistical physics and probabilistic graphical models. *Journal of Physics A: Mathematical and General*, 38(33):R309, 2005.
- [40] J. Peng, T. Hazan, N. Srebro, and J. Xu. Approximate inference by intersecting semidefinite bound and local polytope. In Artificial Intelligence and Statistics, pages 868–876. PMLR, 2012.
- [41] Y. Peng, S. Yang, Y. Khoo, and D. Wang. Tensor density estimator by convolution-deconvolution. arXiv preprint arXiv:2412.18964, 2024.
- [42] G. Peyré, M. Cuturi, et al. Computational optimal transport: With applications to data science. Foundations and Trends® in Machine Learning, 11(5-6):355-607, 2019.
- [43] J. Rabin, G. Peyré, J. Delon, and M. Bernot. Wasserstein barycenter and its application to texture mixing. In *International conference on scale space and variational methods in computer vision*, pages 435–446. Springer, 2011.
- [44] C. Scarvelis and J. Solomon. Riemannian metric learning via optimal transport. In *International Conference on Learning Representations*. OpenReview, 2023.
- [45] D. Sun, K.-C. Toh, Y. Yuan, and X.-Y. Zhao. Sdpnal+: A matlab software for semidefinite programming with bound constraints (version 1.0). *Optimization Methods and Software*, 35(1):87–115, 2020.
- [46] T. Tang and K.-C. Toh. Exploring chordal sparsity in semidefinite programming with sparse plus low-rank data matrices. arXiv preprint arXiv:2410.23849, 2024.
- [47] I. Tolstikhin, O. Bousquet, S. Gelly, and B. Schoelkopf. Wasserstein auto-encoders. arXiv preprint arXiv:1711.01558, 2017.
- [48] L. N. Trefethen. Approximation theory and approximation practice, extended edition. SIAM, 2019.
- [49] A. Vacher, B. Muzellec, A. Rudi, F. Bach, and F.-X. Vialard. A dimension-free computational upper-bound for smooth optimal transport estimation. In *Conference on Learning Theory*, pages 4143–4173. PMLR, 2021.
- [50] C. Villani. Topics in optimal transportation, volume 58. American Mathematical Soc., 2021.
- [51] C. Villani et al. Optimal transport: old and new, volume 338. Springer, 2008.
- [52] M. J. Wainwright, M. I. Jordan, et al. Graphical models, exponential families, and variational inference. Foundations and Trends® in Machine Learning, 1(1–2):1–305, 2008.
- [53] J. Weed and F. Bach. Sharp asymptotic and finite-sample rates of convergence of empirical measures in wasserstein distance. *Bernoulli*, 25(4A):2620–2648, 2019.

[54] J. Weed and Q. Berthet. Estimation of smooth densities in wasserstein distance. In conference on Learning Theory, pages 3118–3119. PMLR, 2019.